Tuning the electronic structure of MoMo quadruple bonds by N for O for S substitution

Jamie Hicks, Sam Ring and Nathan J. Patmore*

The University of Sheffield, Department of Chemistry, Sheffield, S3 7HF, UK

Email: n.patmore@sheffield.ac.uk

Abstract

A series of quadruply bonded dimolybdenum compounds of form $Mo_2(EE'CC{\equiv}CPh)_4$ (EE' = $\{NPh\}_2$, **Mo_2NN**; {NPh}O, **Mo_2NO**;{NPh}S, **Mo_2NS**; OO, **Mo_2OO**) have been synthesised by ligand exchange reactions of $Mo_2(O_2CCH_3)_4$ with the acid or alkali metal salt of $\{PhC{\equiv}CCEE'\}^-$. The compounds **Mo_2NO**, **Mo_2NS** and **Mo_2OO** were structurally characterised by single crystal X-ray crystallography. The structures show that **Mo_2NO** adopts a *cis*-2,2 arrangement of the ligands about the Mo_2^{4+} core, whereas **Mo_2NS** adopts the *trans*-2,2 arrangement. The influence of heteroatom substitution on the electronic structure of the compounds was investigated using cyclic voltammetry and UV/vis spectroscopy. Simple N for O for S substitution in the bridging ligands significantly alters the electronic structure, lowering the energy of the Mo_2-δ HOMO and reducing the $Mo_2^{4+/5+}$ oxidation potential by up to 0.9 V. A different trend is found in the optoelectronic properties, with the energy of the Mo_2-δ-to-ligand-π^* transition following the order **Mo_2OO > Mo_2NO > Mo_2NN > Mo_2NS**. Electronic structure calculations employing density functional theory were used to rationalise these observations.

Introduction

Quadruply bonded dimetal compounds of form $M_2(\mu\text{-}L)_4$ (L = bidentate, three atom, bridging ligand; M = Mo, W) have a paddlewheel arrangement of the ligands about the dimetal core, and two axial sites that can be used to coordinate exogenous ligands.[1] The M_2^{4+} core has a $\sigma^2\pi^4\delta^2$ electronic configuration, and a wide variety of bridging ligands, such as carboxylate and formamidinate, have been employed to support the dimetal core. The utility of the redox active quadruple bond was illustrated by $W_2(hpp)_4$ (Hhpp = 1,3,4,6,7,8-hexahydro-2*H*-pyrimido[1,2-*a*]pyrimidine), which is the most easily ionised closed-shell molecule known and a powerful reducing agent.[2, 3] In addition, Berry and co-workers have shown that the ditungsten core of W_2(2,2'-dipyridylamide)$_4$ is capable of undergoing a four-electron oxidation process which, remarkably, is chemically reversible.[4] The redox potential of dimolybdenum paddlewheel compounds has also been found to play an important role in their performance as catalysts in radical addition and polymerisation reactions.[5] Mixed-valence 'dimers of dimers' of the type $[M_2](\mu\text{-}O_2C\text{-}X\text{-}CO_2)[M_2]^+$ (M = Mo, W), where X a conjugated spacer, are particularly suited for the study of electron transfer processes[6] and have been extensively studied over the past couple of decades as strong electronic coupling is observed between the dimetal units.[7-15] The coupling is mediated by M_2-δ to bridge-π conjugation and is dependent on the nature of the bridging ligand and metal employed.

More recent studies have shown that MM multiply bonded paddlewheels have remarkably long lived excited state lifetimes.[16, 17] Investigations by Chisholm and coworkers on the photoexcited states of *trans*-$[M_2(TiPB)_2(O_2CR)_2]$ (R = 2-thiophene[18, 19] or C_6H_4-4-CN; TiPB = 2,4,6-triisopropylbenzoate)[20] show emission from T_1 states that are $^3MM\delta\delta^*$ in nature when M = Mo (τ = 77 or 93 μs), but ^{3}MLCT

in nature when M = W (τ = <10 ns). The well-defined coordination environment about the dimetal core also makes MM multiply bonded paddlewheel compounds good candidates for incorporation into materials with potentially interesting optoelectronic properties.[21-27] This was highlighted in a detailed study by Zhou and co-workers which demonstrated that the shape and size of molecular architectures formed using dicarboxylate ligands to bridge Mo_2^{4+} units can be controlled by tuning the bridging angle and size of the bridging dicarboxylate ligand.[28]

Changing the nature of the three atom ligand bridging the M_2^{4+} core has been found to have a marked effect on the properties of this type of compound.[29, 30] The substitution of O for S in $[L_3Mo_2]_2(\mu$-1,4-(EE'C)$_2$-C_6H_4) (EE' = OO, OS, SS; L = O_2CBu^t or *N,N'*-di-*p*-anisylformamidinate) results in a decrease of the HOMO (M_2-δ) - LUMO (bridge π^*) energy gap, and a greater mixing of the metal- and bridge-based orbitals which gives rise to a significant increase in electronic coupling.[31, 32] Similar reasoning was used to account for the increases in electronic coupling observed when thiooxamidate as opposed to oxamidate is used to bridge Mo_2 quadruply bonded units.[33] The M_2^{4+} bridging ligand has also been shown to have an effect on the nature of the excited states;[18] the ^{3}MLCT of *trans*-$[W_2(TiPB)_2(L)_2]$ is localised on one ligand when L is an amidinate (L = N(^{i}Pr)$_2$CC≡CPh), but delocalised over both ligands for a carboxylate (L = $O_2CC_6H_4$-4-CN).[20]

Despite the often dramatic effect that changing the bridging atoms of the bridging ligand has on the electronic structure and properties of quadruply bonded paddlewheel compounds, there have been no systematic studies as to the origins of these effects. Here we report the synthesis of a series of compounds of form Mo_2(EE'CC≡CPh)$_4$ (EE' = {NPh}$_2$, {NPh}O, {NPh}S, OO), shown in Scheme 1. The effect of substitution of N for O for S on the electronic structure of the dimetal core and

conjugation between the Mo_2-δ and ligand-π orbitals was investigated using UV/vis spectroscopy, electrochemistry and X-ray diffraction studies, which are correlated with the results from density functional theory (DFT) calculations.

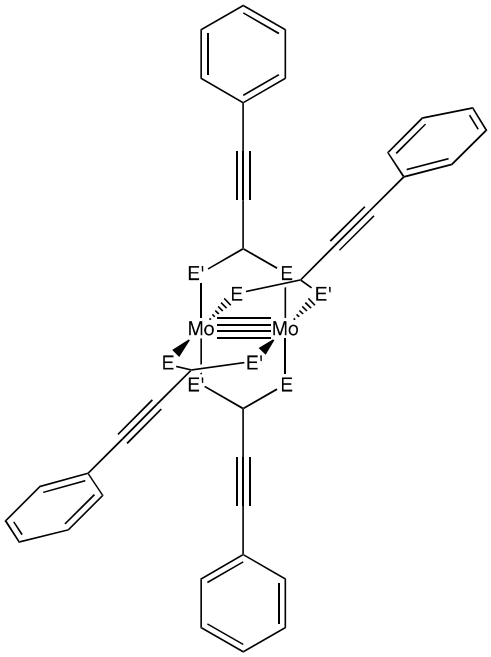

Scheme 1. Drawing of the complexes used in this study.

Results and discussion

Synthesis

The compounds $Mo_2(\{NPh\}_2CC{\equiv}CPh)_4$ (**Mo_2NN**), $Mo_2(\{NPh\}C(O)C{\equiv}CPh)_4$ (**Mo_2NO**), $Mo_2(\{NPh\}C(S)C{\equiv}CPh)_4$ (**Mo_2NS**), and $Mo_2(O_2CC{\equiv}CPh)_4$ (**Mo_2OO**) were all prepared by ligand substitution reactions with $Mo_2(O_2CCH_3)_4$. The reaction conditions are summarised in Scheme 2, with some procedures requiring use of the alkali metal salt or elevated temperatures to ensure complete substitution of the acetate ligands in the dimolybdenum starting material.

The solubility of the compounds varied significantly depending on the nature of the ligand employed; **Mo_2NN** and **Mo_2NS** are soluble in most organic solvents, **Mo_2OO** is soluble in weak donor solvents such as THF, whilst **Mo_2NO** is only soluble in

strong donor solvents such as DMSO or DMF. All compounds gave satisfactory elemental analysis and show the molecular ions M^+ by matrix assisted laser desorption/ionization time-of-flight (MALDI-TOF) mass spectrometry. The ^{1}H NMR spectra of the compounds all display overlapping aromatic resonances associated with the ligand phenyl groups.

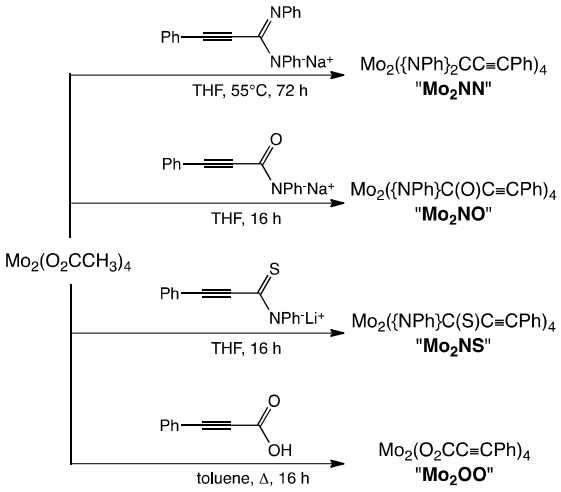

Scheme 2. Reaction conditions for the synthesis of compounds **Mo_2NN**, **Mo_2NO**, **Mo_2NS** and **Mo_2OO**.

The yield of **Mo_2NN** was consistently low, and MALDI-TOF-MS analysis of the crude reaction mixture showed a mixture of product and a molecular ion consistent with the formation of a $(PhC{\equiv}CC\{NPh\}_2)_3Mo_2(\mu\text{-}OH)_2Mo_2(\{NPh\}_2CC{\equiv}CPh)_3$ by-product, presumably from reaction of the product with adventitious H_2O.[34, 35] However, the product could be extracted cleanly from this mixture using warm hexane.

The synthesis of the dithiocarboxylate and monothiocarboxylate compounds $Mo_2(S_2CC{\equiv}CPh)_4$ and $Mo_2(OC(S)C{\equiv}CPh)_4$ was also attempted. Reaction of $Mo_2(O_2CCH_3)_4$ with the alkali salt of the ligand[36] prepared *in situ* in THF at -78°C resulted in the formation of a green solution. Upon warming to room temperature, the

solutions turns a dark black colour above -10°C, and removal of the solvent yields a black oil in both instances. No evidence of any dimolybdenum ions were found in the mass spectra of these oils, and the thermal instability of the initial green solution precluded further analysis.

For the compounds **Mo_2NO** and **Mo_2NS** there are 4 possible regioisomers, depicted in Scheme 3. Isomerisation of dimolydenum paddlewheel compounds in solution can be studied by ^{1}H NMR spectroscopy,[37] although in the case of **Mo_2NO** and **Mo_2NS** overlap of the phenyl proton resonances precluded a variable temperature ^{1}H NMR study of potential isomeric forms in solution. In the ^{13}C{^{1}H} NMR spectrum of **Mo_2NO** and **Mo_2NS**, only one N-*C*-E resonance was observed demonstrating that one isomeric form is present in solution at room temperature. There is insufficient information in the NMR spectra to assign which regioisomer is present in solution, however it is reasonable to assume that the regioisomers observed in the solid-state studies, *vide infra*, persist in solution.

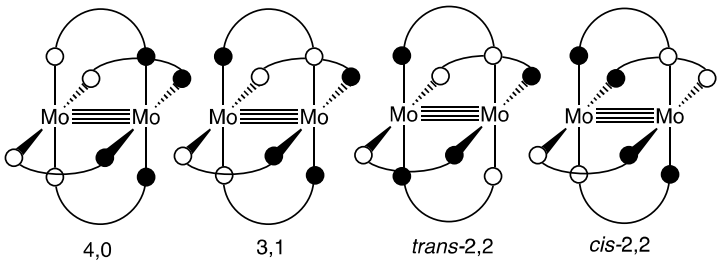

Scheme 3. Possible regioisomers for **Mo_2NO** and **Mo_2NS**.

Solid state structures

Despite numerous attempts, we were unable to obtain crystals of **Mo_2NN** suitable for X-ray diffraction studies. Crystals were obtained for the compounds **Mo_2NO** (Figure 1), **Mo_2NS** (Figure 2) and **Mo_2OO** (Figure 3). Selected bond lengths and angles for

all compounds are displayed in Table 1. The molecule **Mo_2NO** lies about an inversion centre, and there are two independent Mo_2^{4+} units present in the solid state structure of **Mo_2NS**, which lie at sites with crystallographically imposed 2-fold symmetry; a drawing of the second molecule is given in the supporting information.

All compounds display the expected paddlewheel arrangement of the ligands about the dimetal core. The solid-state structure of **Mo_2NO** reveals a *cis*-2,2 arrangement of the ligands, where as **Mo_2NS** adopts the *trans*-2,2 regioisomer.

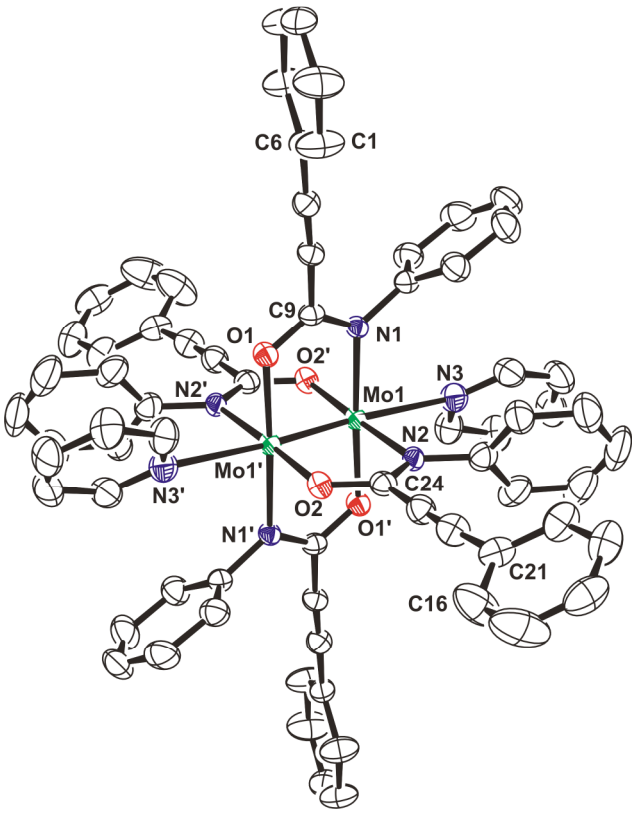

Figure 1. Solid state structure of **Mo_2NO**$(py)_2$, with anisotropic displacement parameters drawn at the 50% level and hydrogen atoms omitted for clarity. Atoms with an additional prime (') character are generated using the symmetry operation 1-x, -y, 1-z.

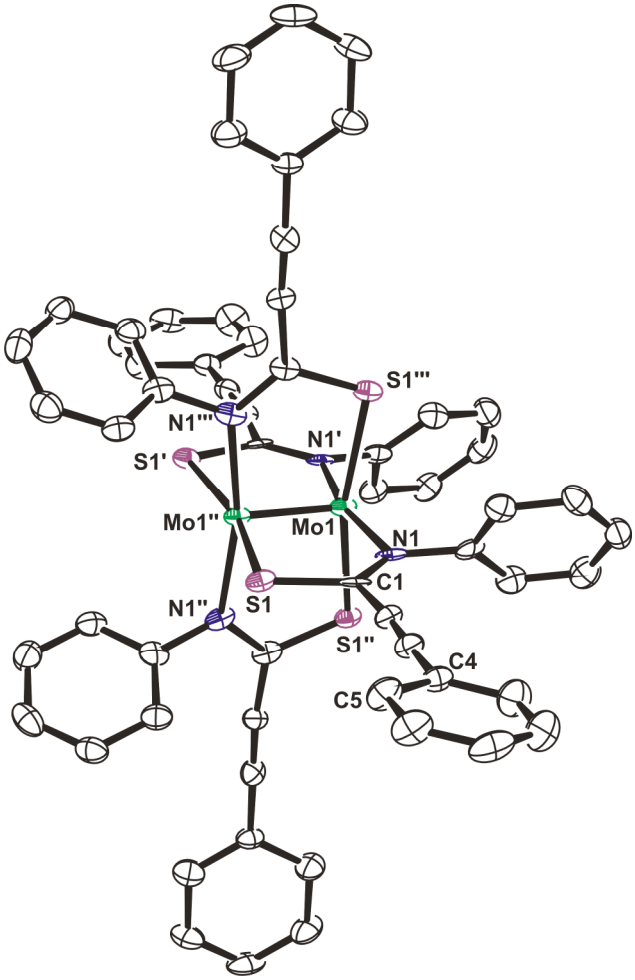

Figure 2. Solid state structure of one of the crystallographically independent cores of **Mo_2NS**, with anisotropic displacement parameters drawn at the 50% level and hydrogen atoms omitted for clarity. Atoms with a prime ('), double prime (") and triple prime ("') character are generated using the symmetry operations '1-x, 1-y, z', 'y, 1-x, 2-z' and '1-y, x, 2-z', respectively.

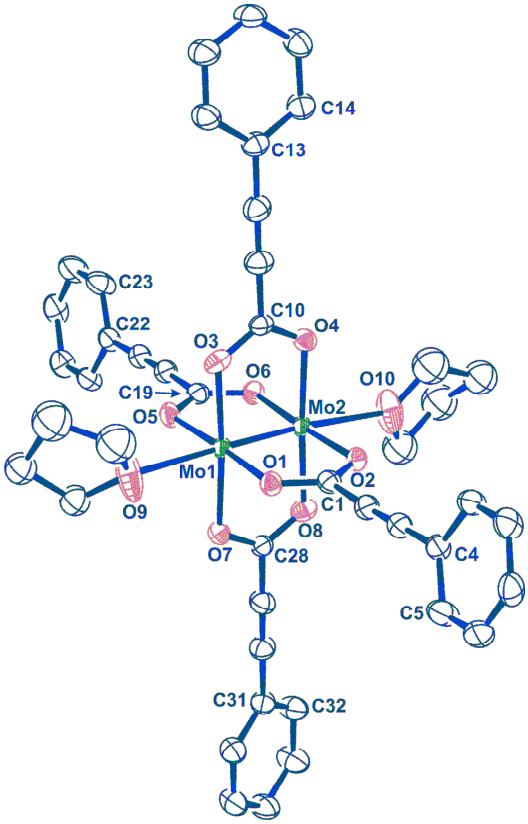

Figure 3. Solid state structure of **Mo_2OO**$(THF)_2$. Anisotropic displacement parameters are drawn at the 50% level, with hydrogen atoms have been omitted for clarity.

Table 1. Selected bond lengths (Å) and angles (º) for **Mo_2NO**$(py)_2$, **Mo_2NS**, and **Mo_2OO**$(THF)_2$

	Mo_2NO $(py)_2$	**Mo_2NS**	**Mo_2OO**$(THF)_2$	
Mo-Mo	Mo1-Mo1' 2.1269(7)	Mo1-Mo1'' 2.1026(18) Mo2-Mo2''' 2.1171(16)	Mo1-Mo2 2.1106(6)	
Mo-L_{eq}	Mo1-N1 2.136(3) Mo1-N2 2.141(3) Mo1-O1 2.111(2) Mo1-O2 2.114(2)	Mo1-N1 2.149(6) Mo1-S1'' 2.462(2) Mo2-N2 2.144(6) Mo2-S2'' 2.457(2)	Mo1-O1 2.107(4) Mo1-O3 2.100(4) Mo1-O5 2.101(4) Mo1-O7 2.094(4)	Mo2-O2 2.101(4) Mo2-O4 2.092(4) Mo2-O6 2.117(4) Mo2-O8 2.114(4)
Mo-L_{ax}	Mo1-N3 2.690(3)	-	Mo1-O9 2.540(6)	Mo2-O10 2.558(6)
Phenyl torsion	O1'-C9-C6-C1 72.7(4) O2'-C24'-C21'-C16' 29.9(5)	S1-C1-C4-C5 10.9(7) S2-C16-C19-C20 72.2(7)	O1-C1-C4-C5 70.6(6) O4-C10-C13-C14 1.3(6)	O6-C19-C22-C23 80.3(6) O8-C28-C31-C32 21.4(6)

The Mo-Mo bond distance for **Mo_2NO** (2.1269(7) Å) is the longest bond length found for a homoleptic dimolybdenum quadruply bonded compound containing N-C-O^- bridging ligands. The metal-metal distance for **Mo_2OO** (2.1106(6) Å) is also relatively long for a complex of form $Mo_2(O_2CR)_4(THF)_2$; only $Mo_2(O_2CCF_3)_4(THF)_2$ has a longer Mo-Mo bond distance (2.1202(5) Å).[38] The relatively long Mo-Mo bond lengths observed for both compounds may be a result of significant Mo_2-δ to ligand-π^* backbonding.

There have been only four structural studies of dimolybdenum paddlewheel compounds containing bridging N-C-S^- units, using the ligands $^-SC(NMe)PMe_2$ (Mo-Mo = 2.083(1) Å),[39] 4,6-dimethyl-2-mercaptidopyrimidine (Mo-Mo = 2.083(2) Å),[40] 7-methyl-1,8-napthyridine-2-thiolate (Mo-Mo = 2.131(2) Å) and 2-mercaptidoquinoline (Mo-Mo = 2.089(1) Å). The Mo-Mo bond lengths for the two independent molecules in the crystal structure of **Mo_2NS** are slightly different (2.1026(18) and 2.1171(16) Å), but fall within the range observed for other Mo_2^{4+} cores with N-C-S^- bridging ligands. The only significant difference is the orientation of the phenyl ring on the ligand backbone; the torsion angles with the N-C-S^- moiety and phenyl rings are 10.9(7)° and 72.2(7)°.

Electrochemical studies

The cyclic voltammograms of **Mo_2NN**, **Mo_2NO**, **Mo_2NS**, and **Mo_2OO** are displayed in Figure 4, with data summarised in Table 3. All compounds display a single oxidation process corresponding to the removal of an electron from the highest occupied molecular orbital (HOMO), which is the Mo_2-δ orbital. The $Mo_2^{4+/5+}$ redox process is reversible for **Mo_2NS** in THF solution, and **Mo_2NN** in dichloromethane and dimethylformamide. However this process is irreversible for all compounds, except **Mo_2NN**, in dimethylformamide. In solutions containing dimolybdenum paddlewheel compounds, donor solvents will coordinate to the axial sites of the Mo_2 core. The irreversible nature of the oxidation in dimethylformamide is likely a result of attack of the M-M bond in the Mo_2^{5+} ions formed by the axially coordinated donor solvent molecules. The small change observed in oxidation potential for **Mo_2NN** in dimethylformamide (-0.322 V) and dichloromethane solutions (-

0.313 V) suggests that the ligand *N*-phenyl groups protect the axial coordination site of the dimetal core from dimethylformamide coordination, accounting for the reversible nature of the $Mo_2^{4+/5+}$ redox process.

The trend in oxidation potentials (**Mo_2NN < Mo_2NO < Mo_2NS < Mo_2OO**) correlate with ligand basicity; the more basic the ligand the better the stabilisation of the Mo_2^{5+} oxidation state. Hence the lowest oxidation potential is observed for **Mo_2NN**, whilst **Mo_2OO** has the highest. The range of the Mo_2^{4+}/Mo_2^{5+} potentials (~0.9 V) illustrates the dramatic effect that the character of the ligand bridging atoms has on the electronic structure of these compounds.

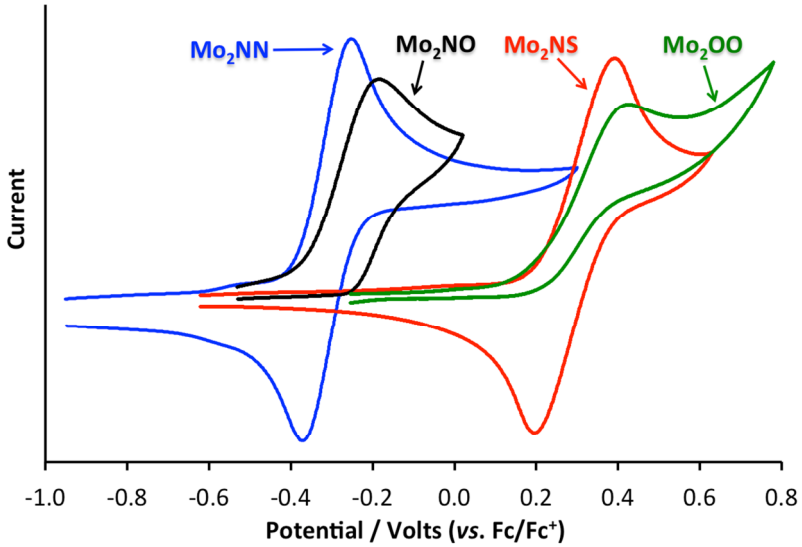

Figure 4. Cyclic voltammograms of **Mo_2NN** (in dichloromethane), **Mo_2NO** (in dimethylformamide), **Mo_2NS** (in THF) and **Mo_2OO** (in THF) recorded in 0.1 M $^{n}Bu_4NPF_6$ solutions.

Electronic absorption spectroscopy

The UV/vis absorption spectra of the compounds are shown in Figure 5. All compounds show an intense absorption in the visible region, which can be assigned to Mo_2 $\delta \rightarrow$ ligand π^* (MLCT) transitions. The energy of this transition is dependent on the nature of the ligand. The highest energy MLCT transition is observed for **Mo_2OO** at 446 nm, with the same transition red shifted for

Mo_2NO (496 nm), **Mo_2NN** (520 nm) and **Mo_2NS** (526 nm). The compound **Mo_2NO** also displays a weak transition at 605 nm. A more detailed analysis of these transitions can be obtained from the time-dependent density functional theory calculations, discussed next.

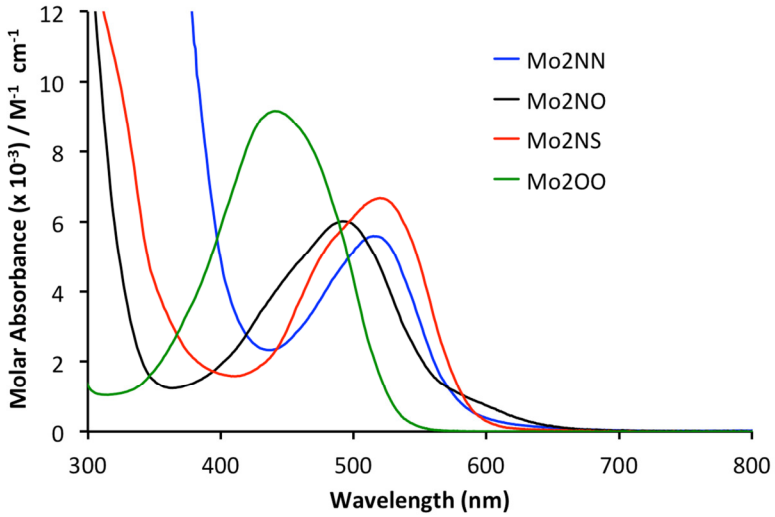

Figure 5. UV/vis spectra of **Mo_2NN**, **Mo_2NO**, **Mo_2NS** and **Mo_2OO** recorded in DMF solutions at room temperature.

Electronic structure calculations

The geometry and electronic structures of all the compounds were studied by density functional theory calculations as implemented in the Gaussian09 suite of programs.[41] The model compounds Mo_2({NH}$_2$CC≡CPh)$_4$ (**Mo_2NN'**), Mo_2({NH}C(O)C≡CPh)$_4$ (**Mo_2NO'**) and Mo_2({NH}C(S)C≡CPh)$_4$ (**Mo_2NS'**), in which {NPh} has been replaced by {NH}, were used to reduce computational time. Whilst the compounds Mo_2(SC(O)C≡CPh)$_4$ (**Mo_2SO**) and Mo_2(S_2CC≡CPh)$_4$ (**Mo_2SS**) could not be isolated in this study due to their instability at room temperature, homoleptic dimolybdenum monothio- and dithiocarboxylate paddlewheel compounds are known.[42] Calculations were therefore also performed on **Mo_2SO** and **Mo_2SS** as it is informative to consider the effect of sulphur coordination on the electronic structure. Selected bond lengths for the optimised structures are given in Table 2, and show excellent agreement with the solid state structures obtained for **Mo_2NS**, **Mo_2OO** and **Mo_2NO**.

Table 2. Calculated bond lengths (Å).

	Mo_2NN'	**Mo_2NO'**	**Mo_2NS'**	**Mo_2OO**	**Mo_2SO**	**Mo_2SS**
Mo-Mo	2.137	2.130	2.142	2.124	2.156	2.150
Mo-N	2.149	2.140	2.140	-		
Mo-O	-	2.107	-	2.104	2.078	
Mo-S	-	-	2.506	-	2.495	2.496

Regioisomers

We first probed which regioisomers of **Mo_2NO'**, **Mo_2NS'** and **Mo_2SO** are more stable in the gas phase by optimising the structures of the 4,0, 3,1, *trans*-2,2, and *cis*-2,2 regioisomers (see Scheme 3). The results shown in Figure 6 indicate that the *trans*-2,2 regioisomer is the most stable in all instances. For **Mo_2NO'** and **Mo_2SO**, there are a number of regioisomers close (<5 kJ mol^{-1}) in energy to the *trans*-2,2 form. This suggests that more than one regioisomer could be present in the solid-state or at elevated temperatures in solution, although no experimental evidence of multiple regioisomers was observed. The solid state structure of **Mo_2NO** it was found to adopt the *cis*-2,2 regioisomer. As this is the only form observed experimentally, subsequent discussion about **Mo_2NO'** will focus on results from the *cis*-2,2 isomer calculations. For **Mo_2NS'** and **Mo_2SO'**, the results of the *trans*-2,2 isomer calculations will be discussed.

In order to check that substitution of {NH} for {NPh} did not affect the relative stability of the isomers, geometry optimisation on the *cis*-2,2 and *trans*-2,2 forms of **Mo_2NO** were performed; the *trans*-2,2 isomer was still found to be the most stable.

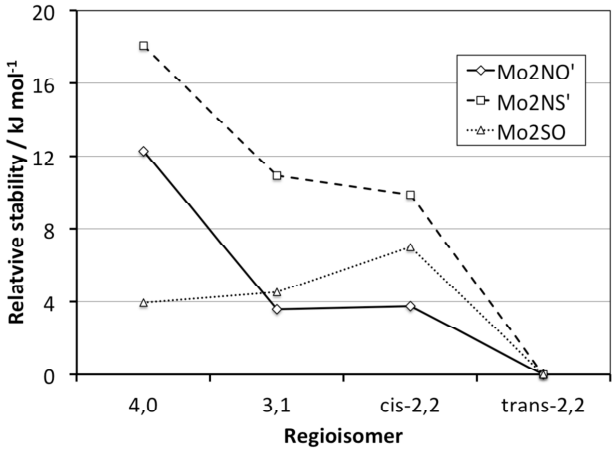

Figure 6. Calculated stabilities of isomeric forms of **Mo_2NO'**, **Mo_2NS'** and **Mo_2SO**.

Electronic Structure

The calculated frontier molecular orbital energy levels and selected MO diagrams for **Mo_2OO** are displayed in Figure 7. The HOMO in all instances is the Mo_2 δ, with energies given in Table 3 ranging from -3.83 eV for **Mo_2NN** to -5.26 eV for **Mo_2SS**. This large energy range of ~1.4 eV shows that substitution of N for O for S can result in dramatic changes in the electronic structure of dimolybdenum paddlewheel compounds. This effect is even greater than would be expected if Mo was substituted by W, which would result in the M_2-δ orbital rising by ~0.5 eV in energy.[43] The electrochemical data is also included in Table 3, and shows that the calculated trend in HOMO energy is matched by experiment.

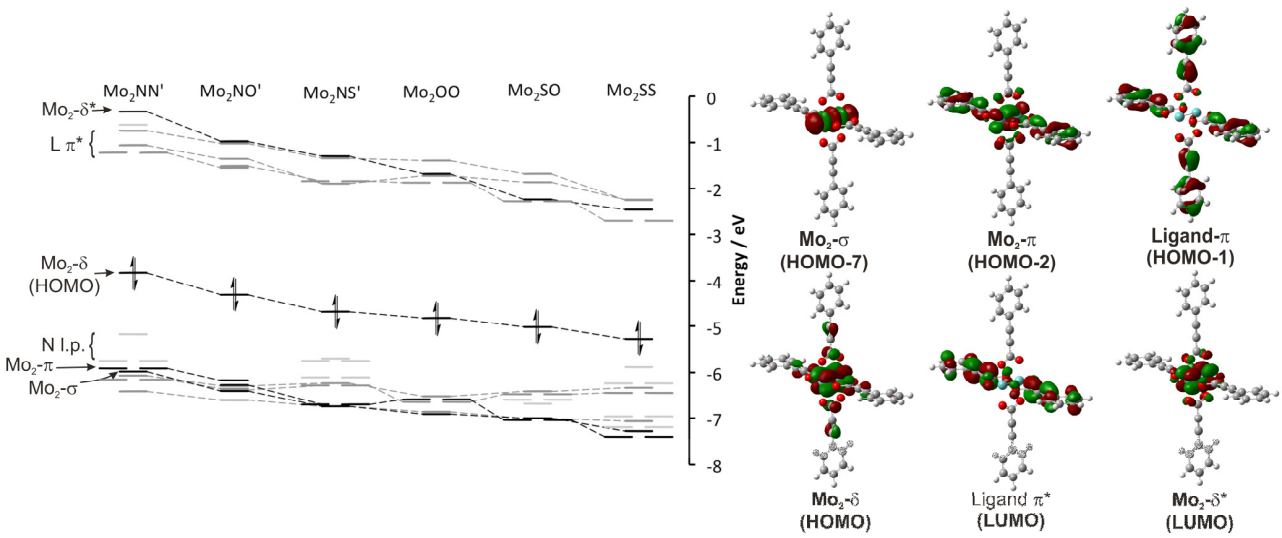

Figure 7. Calculated frontier molecular orbital energies and selected Gaussview plots of Mo_2OO orbitals (drawn with an isosurface value of 0.03).

Table 3. Calculated MO energies, and a comparison of the experimental observed and calculated energy of the MLCT transition.

Compound	**HOMO / eV[a]**	**HOMO-LUMO gap / eV[a]**	**$\Delta E(L\pi^*)$ / eV[a]**	**$E_{1/2}(1)$ / V[b,c]**	**λ_{max} obs (ε) /nm (M^{-1} cm^{-1})[c]**	**λ_{max} calc /nm[a]**	**λ_{max} calc assignment**
Mo_2NN	-3.83	2.62	0.46	-0.322 (–0.313[d])	520 (5600)	539 (1.564)	$\delta \rightarrow L\pi^*$
Mo_2NO	-4.31	2.77	0.52	–0.200[e]	605 (600) 496 (6000)	523 (0.545) 504 (0.778) 476 (0.216)	$\delta \rightarrow L\pi^*$ $\delta \rightarrow L\pi^*$ $\delta \rightarrow \delta^*$
Mo_2NS	-4.68	2.79	0.55	0.092[e] (0.297[f])	526 (6600)	508 (1.300) 468 (0.138)	$\delta \rightarrow L\pi^*$ $\delta \rightarrow M_2\text{-}\pi^*$
Mo_2OO	-4.82	2.95	0.49	0.282[e] (0.410[e,f])	446 (9100)	484 (1.560)	$\delta \rightarrow L\pi^*$
Mo_2SO	-5.02	2.74	0.60	-	-	527 (1.297)	$\delta \rightarrow L\pi^*$
Mo_2SS	-5.27	2.56	0.45	-	-	570 (1.064) 421 (0.302)	$\delta \rightarrow L\pi^*$ S l.p. $\rightarrow L\pi^*$

a) Calculated values. b) *vs*. $Cp_2Fe^{0/+}$. c) recorded in dimethylformamide solution. d) recorded in dichloromethane solution. e) irreversible oxidation wave. f) recorded in THF solution.

The LUMO for each compound is one of the ligand π^* orbital combinations, and included in Table 3 is the calculated HOMO-LUMO gap. The effect of N for O for S substitution on the HOMO-LUMO gap is less dramatic than observed for the HOMO energy. Introduction of the more electronegative O for N reduces the energy of the ligand π^* orbitals. The effect of S for N substitution is also to reduce the energy of the ligand π^*, however in this instance it is the longer and weaker C–S bond that is responsible for the reduction in energy. These effects combine to result in similar reduction in the ligand π^* orbital energies as the Mo_2-δ orbitals energies are reduced.

In complexes of the type $M_2(TiPB)_2(L)_2$ (L = π-accepting carboxylate ligand) the separation between the in- and out-of-phase π^* combinations of 'L' can be used as a measure of the strength of interaction between the O_2CR π-systems and the Mo_2-δ.[43] In homoleptic paddlewheel compounds having D_{4h} symmetry, there are three non-bonding ligand π^* combinations of e_u and a_{2g} symmetry, and a b_{2g} combination that has the correct symmetry to interact with the Mo_2-δ. Molecular orbital diagrams of the b_{2g} combination are given in the Supporting Information. The extent of separation between these bonding and non-bonding combinations, $\Delta E(L\pi^*)$, is therefore an indication of the extent of coupling between the M_2-δ and ligand π-systems, with values presented in Table 3. Based on the HOMO-LUMO separation, the magnitude of $\Delta E(L\pi^*)$ would be expected to follow the order **Mo_2NN < Mo_2NO < Mo_2NS**. The reverse of this order is actually observed. This can be rationalised by examining the MO diagrams which show the amount N-C-E π^* character in the ligand π^* orbital follows the trend E = N < O < S. The bridging N-C-E group is serving as an 'alligator clip',[6, 44] coupling metal and ligand π orbitals. The large 3 p orbitals of sulphur have the best overlap, and hence the strongest metal-ligand coupling is observed. This highlights that it is essential to consider metal and E-C-E' orbital overlap, and not just MO energy, when choosing ligands to electronically couple dimetal units.

For **Mo_2SS**, a smaller than expected separation of the ligand π^* orbital combinations is observed. The MO diagram of the b_{2g} ligand π^* combination for **Mo_2SS**, shown in the Supporting Information, reveals additional bonding interactions between the diffuse S 3p orbitals on adjacent ligands are present, which serve to stabilise the orbital.

Time-dependent DFT was used to calculate the absorption spectra for each compound. Calculated transitions with significant oscillator strength ($f > 0.1$) in the visible region are listed in Table 3. In each instance, the main transition in the visible region is the expected Mo_2-δ to ligand π^* transition, with the calculated values closely matching the experimental data. However, they do not predict the weak transition observed at 605 nm for **Mo_2NO**. This peak could be due to a $\delta \rightarrow \delta^*$ transition, which for **Mo_2NO'** is calculated to have appreciable oscillator strength.

Conclusion

This investigation has probed how N for O for S substitution in the E-C-E' bridging group of dimolybdenum quadruply bonded paddlewheel compounds influences their properties. For the $Mo_2(EE'CC{\equiv}CPh)_4$ compounds studied, this simple change was shown to have a dramatic effect on the electronic structure of dimolybdenum core. Electrochemical studies showed that Mo_2^{4+} oxidation can be tuned over a range of nearly 0.9 V, with N for O for S substitution, because of decreases in ligand basicity. Density functional theory calculations indicate that this range could be increased upon inclusion of mono- and di-thiocarboxylate ligands to the series.

Dicarboxylates are by far the most common ligands used in the assembly of molecular architectures incorporating M_2^{4+} units or other metal clusters. This study has shown that the optoelectronic and redox properties of these assemblies may be tuned by judicious selection of bridging ligand. Given that heteroatom substitution has a dramatic effect on the ground-state properties of these molecules, future studies will also investigate differences in the photoexcited states of these compounds.

Experimental

Physical measurements

Elemental analyses were carried out by the Microanalytical Service of the Department of Chemistry at Sheffield with a Perkin-Elmer 2400 analyzer. Electronic absorption spectra were recorded using a Varian Cary 5000 UV-Vis-NIR spectrophotometer. Electrochemical measurements were carried out in nitrogen-purged 0.1 M [$^{n}Bu_4N$][PF_6] solutions using a standard three-electrode system with a Pt microdisc working electrode, Pt wire counter electrode, and Ag/AgCl reference electrodes. At the end of every experiment ferrocene was added as an internal standard. ESI mass spectra were collected on a Waters Micromass LCT operating in ESI mode. Matrix assisted laser desorption/ionisation time-of-flight (MALDI-TOF) mass spectrometry was performed on a Bruker Reflex III (Bruker, Breman, Germany) mass spectrometer operated in positive ion mode with a N2 laser. Laser power was used at the threshold level required to generate signal. Dithranol was used as the matrix and prepared as a saturated solution in THF. Allotments of matrix and sample were thoroughly mixed together; 0.5 mL of this was spotted on the target plate and allowed to dry. IR spectra were recorded as solid samples with a Perkin-Elmer Spectrum RX I FT-IR spectrometer equipped with a DuraSamplIR II diamond ATR probe and universal press. ^{1}H and ^{13}C NMR spectra were collected at room temperature on Bruker Avance 250, 400 or DRX500 spectrometers. Chemical shifts were assigned relative to the residual solvent peak and are given to 0.01 ppm for ^{1}H and 0.1 ppm for ^{13}C.

Materials and methods

All experimental manipulations were performed under an inert atmosphere using standard Schlenk-line and glovebox techniques. THF was distilled over sodium wire, and methanol was distilled over CaH_2. All other solvents obtained from a “Grubbs” solvent purification system. *N,N’*-diphenyl carbodiimide (PhN=C=NPh),[45] PhC≡C(O)CNHPh,[46] and $Mo_2(O_2CCH_3)_4$[47] were synthesised according to literature procedures. All other chemicals were obtained from commercial sources.

Preparation of PhC≡C(NPh)CN(H)Ph

This ligand was synthesised by a modified literature procedure.[48] Phenyl acetylene (0.272 g, 2.66 mmol) was dissolved in THF (20 ml) and cooled to -78°C. *n*-Butyllithium (1.06 ml of a 2.5M solution in hexane, 2.66 mmol) was added slowly to the solution and stirred for 20 min at -78°C. A solution of freshly prepared and degassed *N,N'*-diphenyl carbodiimide (0.486 g, 2.50 mmol) was dissolved in THF (10 ml) and added dropwise. The pale yellow solution was allowed to warm slowly to room temperature and stirred for 2 h, producing a further colour change to orange. The reaction was quenched by addition of MeOH (25 ml), and the solvent removed to leave a yellow solid. The solid was purified by recrystallisation from hot hexane to yield orange needle crystals (0.652 g, 88%). ^{1}H NMR ($CDCl_3$, 20°C): δ 8.06 (s, 1H, *N*H), 7.77-7.29 (m, 15H, *Ar*H). $^{13}C\{^{1}H\}$ NMR ($CDCl_3$, 20°C): 80.6 (Ar-*C*≡C); 92.7 (Ar-C≡*C*); 120.7, 121.2, 123.3, 128.5, 128.7, 129.8, 132.2, 139.4 (Aryl C); 146.0 (N=*C*(C)N). mp 121°C (lit.,[48] 122-123.5°C). ESI-MS: calcd monoisotopic MW for $C_{21}H_{16}N_2$, 296.1; found m/z 297.1 (MH^+, 100.0%).

Preparation of Mo_2({NPh}$_2$CC≡CPh)$_4$, Mo_2NN

A mixture of sodium hydride (17 mg, 0.70 mmol) and PhC≡C(NPh)CNHPh (207 mg, 0.70 mmol) in THF (15 ml) were heated to 60°C for 15 mins, where upon an orange solution was formed. The solution was then cooled to -78°C and a solution of $Mo_2(O_2CCH_3)_4$ (50 mg, 0.12 mmol) in THF (5 ml) was added dropwise. After addition, the reaction mixture was heated to 55°C, and stirred at this temperature for 72 h. The reaction was then cooled to room temperature, and solvent removed *in vacuo* to leave a dark red solid. The product was extracted from this residue using warm (50°C) hexane, and filtered before drying *in vacuo* to yield a bright red solid (52 mg, 32% yield). Anal. calcd for $C_{84}H_{60}N_8Mo_2$: C, 73.46; H, 4.40; N, 8.16. Found: C, 73.82; H, 4.46; N, 8.09%. MALDI-TOF-MS: calcd monoisotopic MW for $C_{84}H_{60}N_8Mo_2$, 1376.3; found m/z 1376.1 (M^+, 100%). ^{1}H NMR ($CDCl_3$, 20°C): δ7.55-7.02 (m, 60H, *Ar*H). $^{13}C\{^{1}H\}$ NMR($CDCl_3$, 20°C): δ 83.3 (Ar-*C*≡C);

92.6 (Ar-C≡*C*); 120.6, 123.6, 125.46, 128.5, 128.4, 128.7, 131.9, 139.2 (Aryl C); 149.9 (N=*C*(C)N). UV-Vis (DMF) [λ_{max}, nm (ε, M^{-1} cm^{-1})]: 517 (5590).

Preparation of Mo_2(OC{NPh}C≡CPh)$_4$, Mo_2NO

Sodium hydride (0.042 g, 1.8 mmol) and PhC≡CC(O)NHPh (0.388 g, 1.8 mmol) were suspended in THF (20 ml) and heated to 60°C for 15 min. The orange solution that formed was then cooled to -78°C and a solution of $Mo_2(O_2CCH_3)_4$ (0.150 g, 0.35 mmol) in THF (5 ml) was added dropwise. The mixture was stirred at room temperature for 16 hours producing a solution with an orange suspension. The precipitate was isolated by filtration and washed with THF (3 × 10 ml aliquots) before drying *in vacuo* to yield the product as a bright orange solid (250 mg, 67% yield). Crystals suitable for X-ray diffraction were grown by slow diffusion of Et_2O into a pyridine solution containing **Mo_2NO**. Anal. calcd for $C_{60}H_{40}N_4O_4Mo_2$: C, 67.17; H, 3.76; N, 5.22. Found: C, 67.37; H, 3.79; N, 5.13%. MALDI-TOF-MS: calcd monoisotopic MW for $C_{60}H_{40}N_4O_4Mo_2$, 1076.1; found m/z 1075.9 (M^+, 100%). ^{1}H NMR (dmso-d_6, 20°C): δ7.79-7.32 (m, 40H, *Ar*H). $^{13}C\{^1H\}$ NMR (dmso-d_6, 20°C): δ 83.5 (Ar-*C*≡C); 87.0 (Ar-C≡*C*); 120.7, 122.1, 124.6, 126.0, 128.3, 129.2, 132.3, 154.6 (Aryl C); 174.7 (O=*C*(C)N). IR(cm^{-1}): 2360w, 2340w, 1573s, 1488m, 1468s, 1438s, 1387s, 1259w, 1200m, 1098w, 1009w, 992w. UV-Vis (DMF) [λ_{max}, nm (ε, M^{-1} cm^{-1})]: 265 (24570), 492 (6010).

Preparation of Mo_2(SC{NPh}C≡CPh)$_4$, Mo_2NS

Phenyl acetylene (0.192 ml, 1.75 mmol) was dissolved in THF and cooled to -78°C. *n*-Butyllithium (0.70 ml of a 2.5 M solution in hexanes, 1.75 mmol) was added to the solution and stirred for 20 mins at -78°C. Phenyl isothiocyanate (0.201 ml, 1.75 mmol) was added dropwise, then the solution was allowed to warm to room temperature and stirred for 1 h producing a dark red solution. The solution was cooled to -78°C and transferred to a Schlenk flask containing a suspension of $Mo_2(O_2CCH_3)_4$ (0.150 g, 0.35 mmol) in THF (10 ml) also held at -78°C. The mixture was allowed

to warm slowly to room temperature, and stirred for 16 h. The solvent was removed *in vacuo* to leave a red solid, which was redissolved in warm toluene (20 ml, 80°C) and filtered whilst hot. The filtrate was allowed to cool slowly to room temperature yielding the product as red-orange crystals, which were isolated by decantation and dried *in vacuo* (0.320 g, 81%). Anal. calcd for $C_{60}H_{40}N_4S_4Mo_2$: C, 63.37; H, 3.55; N, 4.93; S, 11.28. Found: C, 63.82; H, 3.72; N, 4.87; S, 11.27%. MALDI-TOF-MS: calcd monoisotopic MW for $C_{60}H_{40}N_4S_4Mo_2$, 1140.0; found m/z 1140.2 (M^+, 100%). ^{1}H NMR (dmso-d_6, 20°C): δ7.51-7.32 (m, 16H, *Ar*H), 7.29-7.02 (m, 24H, *Ar*H). $^{13}C\{^1H\}$ NMR (dmso-d_6, 20°C): δ 88.5 (Ar-*C*≡C); 95.8 (Ar-C≡*C*); 120.5, 122.2, 123.2, 127.7, 128.7, 130.7, 131.8, 153.8 (Aryl C); 174.7 (S=*C*(C)N). IR(cm^{-1}): 2359s, 2343m, 1589s, 1482m, 1421s, 1274m, 1766w, 1096s, 1070m, 1024m. UV-Vis (DMF) [λ_{max}, nm (ε, M^{-1} cm^{-1})]: 286 (14610), 520 (6680).

Preparation of $Mo_2(O_2CC{\equiv}CPh)_4$, Mo_2OO

Phenylpropiolic acid (0.250 g, 1.71 mmol) and $Mo_2(O_2CCH_3)_4$ (0.100 g, 0.23 mmol) were refluxed in toluene (15 ml) for 16 h. The reaction mixture was cooled to room temperature producing an orange precipitate. This precipitate was isolated by filtration, and washed with toluene (3 × 10 ml aliquots) before drying *in vacuo,* yielding $Mo_2(O_2CC{\equiv}CPh)_4$ as a bright orange powder (0.110 g, 60%). Crystals suitable for X-ray diffraction were grown by slow diffusion of hexane into a THF solution containing **Mo_2OO**. Anal. calcd for $C_{36}H_{20}O_8Mo_2$: C, 55.98; H, 2.61. Found: C, 56.15; H, 2.73%. MALDI-TOF-MS: calcd monoisotopic MW for $C_{36}H_{20}O_8Mo_2$, 775.9; found m/z 775.9 (M^+, 100%). ^{1}H NMR (dmso-d_6, 20°C): δ7.85-7.52 (m, 20H, *Ar*H). $^{13}C\{^1H\}$ NMR (dmso-d_6, 20°C): δ 81.8 (Ar-*C*≡C); 83.7 (Ar-C≡*C*); 118.9, 129.0, 130.9, 132.8 (Aryl C); 183.4 (O=*C*(C)O). IR(cm^{-1}): 2360w, 2343w, 2210m, 2182w, 1492m, 1475s, 1441m, 1386s, 1220m, 986w, 942w. UV-Vis (DMF) [λ_{max}, nm (ε, M^{-1} cm^{-1})]: 265 (19030), 441 (10540).

X-ray Crystallography

Data were collected were measured on a Bruker Smart CCD area detector with Oxford Cryosystems low temperature system. After integration of the raw data and merging of equivalent reflections, an empirical absorption correction was applied (SADABS) based on comparison of multiple symmetry-equivalent measurements.[49] The structures were solved by direct methods (SHELXS-97)[50] and refined by full-matrix least squares on weighted F^2 values for all reflections.[51] All hydrogens were included in the models at calculated positions using a riding model with U(H) = 1.5 x U_{eq} (bonded carbon atom) for methyl and hydrogens and U(H) = 1.2 x U_{eq} (bonded carbon atom) for methine, methylene and aromatic hydrogens.

For **Mo$_2$NO**(py)$_2$·5py, pyridine solvate molecule located on the inversion centre is delocalised over two positions with site occupancy 0.5/0.5. Two other solvate molecules were disordered over two positions with site occupancies of 0.76/0.24 and 0.52/0.48. The axially coordinated THF molecules in **Mo$_2$OO**(THF)$_2$ are disordered and were refined isotropically over two positions, both with site occupancies of 0.65/0.35. The toluene solvate molecules in **Mo$_2$NS**·4(toluene) are also disordered over two positions with occupancies of 0.51/0.49 and 0.67/0.33, and were refined isotropically. The residual electron density peak of 2.405 e Å^{-3} is located close (1.059 Å) to Mo2.

CCDC 859556 [**Mo2NO**(py)2·5py], 859557 [**Mo2NS**·4(toluene)] and 859558 [**Mo2NS**·4(toluene)] contain the supplementary crystallographic data for this paper. These data can be obtained free of charge from The Cambridge Crystallographic Data Centre via www.ccdc.cam.ac.uk/data_request/cif. Experimental data relating to the structure determinations of all complexes are displayed in Table 4.

Table 4. Crystallographic data for **Mo$_2$NO**(py)$_2$·5py, **Mo$_2$NS**·4(toluene) and **Mo$_2$OO**(THF)$_2$.

Compound	**Mo$_2$NO**(py)$_2$·5py	**Mo$_2$NS**·4(toluene)	**Mo$_2$OO**(THF)$_2$
Empirical Formula	$C_{95}H_{75}Mo_2N_{11}O_4$	$C_{88}H_{72}Mo_2N_4S_4$	$C_{44}H_{36}Mo_2O_{10}$
Formula weight	1626.54	1505.62	916.61
Temperature	100(2) K	150(2) K	150(2) K
Wavelength	0.71073 Å	0.71073 Å	0.71073 Å
Crystal system	Monoclinic	Tetragonal	Monoclinic

Space group	$P2_1/n$	I-4	$P2_1/c$
Unit cell dimensions	a = 13.501(4) Å; α = 90°	a = 26.8014(14) Å; α = 90°	a = 18.8160(6) Å; α = 90°
	b = 20.289(6) Å; β = 90.104(8)°.	b = 26.8014(14) Å; β = 90.104(8)°	b = 12.8292(4) Å; β = 90.032(2)°
	c = 14.126(4) Å; γ = 90°	c = 10.1004(6) Å; γ = 90°	c = 17.2278(5) Å: γ = 90°
Volume	3869(2) Å^3	7255.3(7) Å^3	4158.7(2) Å^3
Z	2	4	4
Density (calculated)	1.396 Mg m^{-3}	1.378 Mg m^{-3}	1.464 Mg m^{-3}
Absorption coefficient	0.387 mm^{-1}	0.511 mm^{-1}	0.659 mm^{-1}
F(000)	1676	3104	1856
θ range for data collection	1.76 to 27.55°.	1.07 to 27.47°	1.08 to 27.50°
Index ranges	-17<=h<=17, -26<=k<=25, -18<=l<=18	-34<=h<=34, -34<=k<=33, -12<=l<=13	-24<=h<=24; -16<=k<=16; -22<=l<=22
Reflections collected	37994	44580	53498
Independent reflections	8876 [R(int) = 0.0464]	8266 [R(int) = 0.0845]	9550 [R(int) = 0.0396]
Completeness to θ	100.0 %	99.6 %	99.8%
Data / restraints / parameters	8876 / 220 / 591	8266 / 27 / 383	9550 / 14 / 499
Goodness-of-fit on F^2	1.181	1.068	1.271
Final R indices [$I > 2\sigma(I)$]	R_1 = 0.0529, wR_2 = 0.1280	R_1 = 0.0556, wR_2 = 0.1276	R_1 = 0.0596, wR_2 = 0.1406
R indices (all data)	R_1 = 0.0708, wR_2 = 0.1399	R_1 = 0.0908, wR_2 = 0.1479	R_1 = 0.0668, wR_2 = 0.1434
Largest diff. peak and hole (e Å^{-3})	0.468 and -0.631	2.405 and -0.901	1.154 and -1.493 e Å^{-3}

Computational details

Molecular structure calculations were performed using density functional theory as implemented in the *Gaussian 09* software package.[41] The B3LYP functional[52, 53] and the 6-31G*(5d) basis set[54] were used for H, C, O, N and S, along with the SDD energy consistent pseudopotentials for molybdenum.[55] This level of theory was chosen as it was recommended in a benchmark study probing the physical and electronic structure of $M_2(O_2CR)_4$ compounds.[56] The model compounds $Mo_2(\{NH\}_2CC{\equiv}CPh)_4$ (**Mo_2NN'**), $Mo_2(\{NH\}C(O)C{\equiv}CPh)_4$ (**Mo_2NO'**) and $Mo_2(\{NH\}C(S)C{\equiv}CPh)_4$ (**Mo_2NS'**), in which {NPh} has been replaced by {NH}, were used. For **Mo_2NS'** and **Mo_2SO** results from calculations on the *trans*-2,2 regioisomer are used in the discussion, and for **Mo_2NO** the discussion is based on computational results from the *cis*-2,2 regioisomer. The structure of each compound was optimised in the gas phase in D_{4h} (**Mo_2NN'**,

Mo_2OO, **Mo_2SS**), D_{2d} (**Mo_2NS'**, **Mo_2SO**) or C_{2h} (**Mo_2NO'**) symmetry, and confirmed to be minima on the potential energy surface using harmonic vibrational frequency analysis. Electronic absorption spectra were calculated using the time-dependent DFT (TD-DFT) method.

Acknowledgements

The Royal Society are thanked for the award of a University Research Fellowship (NJP). S. R. thanks the E-Futures Doctoral Training Centre, a programme funded by the Engineering and Physical Sciences Research Council (EPSRC), for support. Dr Anthony Meijer is thanked for computational assistance and Mr Harry Adams is thanked for crystallographic help.

Supporting Information

A diagram of the second crystallographically independent molecule of **Mo_2NS** and cif files for all structures. Calculated atomic coordinates for all compounds and a molecular orbital plot of the ligand π^* b_{2g} combination for **Mo_2SS**.

References

1. *Multiple Bonds Between Metal Atoms*, 3rd ed., Springer Science and Business Media, Inc, 2005.
2. F. A. Cotton, N. E. Gruhn, J. Gu, P. Huang, D. L. Lichtenberger, C. A. Murillo, L. O. Van Dorn and C. C. Wilkinson, *Science*, 2002, **298**, 1971.
3. F. A. Cotton, J. P. Donahue, D. L. Lichtenberger, C. A. Murillo and D. Villagrán, *J. Am. Chem. Soc.*, 2005, **127**, 10808.
4. M. Nippe, S. M. Goodman, C. G. Fry and J. F. Berry, *J. Am. Chem. Soc.*, 2011, **133**, 2856.
5. H. Tsurugi, K. Yamada, M. Majumdar, Y. Sugino, A. Hayakawa and K. Mashima, *Dalton Trans.*, 2011, **40**, 9358.
6. M. H. Chisholm and N. J. Patmore, *Acc. Chem. Res.*, 2007, **40**, 19.
7. R. H. Cayton and M. H. Chisholm, *J. Am. Chem. Soc.*, 1989, **111**, 8921.
8. R. H. Cayton, M. H. Chisholm, J. C. Huffman and E. B. Lobkovsky, *J. Am. Chem. Soc.*, 1991, **113**, 8709.
9. B. E. Bursten, M. H. Chisholm, R. J. H. Clark, S. Firth, C. M. Hadad, A. M. Macintosh, P. J. Wilson, P. M. Woodward and J. M. Zaleski, *J. Am. Chem. Soc.*, 2002, **124**, 3050.
10. M. V. Barybin, M. H. Chisholm, N. S. Dalal, T. H. Holovics, N. J. Patmore, R. E. Robinson and D. J. Zipse, *J. Am. Chem. Soc.*, 2005, **127**, 15182.
11. M. H. Chisholm, F. Feil, C. M. Hadad and N. J. Patmore, *J. Am. Chem. Soc.*, 2005, **127**, 18150.
12. F. A. Cotton, J. P. Donahue and C. A. Murillo, *J. Am. Chem. Soc.*, 2003, **125**, 5436.

13. F. A. Cotton, J. P. Donahue, C. A. Murillo and L. M. Pérez, *J. Am. Chem. Soc.*, 2003, **125**, 5486.
14. F. A. Cotton, J. P. Donahue, C. Lin and C. A. Murillo, *Inorg. Chem.*, 2001, **40**, 1234.
15. F. A. Cotton, J.-Y. Jin, Z. Li, C. A. Murillo and J. H. Reibenspies, *Chem. Commun.*, 2008, 211.
16. B. G. Alberding, M. H. Chisholm, Y.-H. Chou, J. C. Gallucci, Y. Ghosh, T. L. Gustafson, N. J. Patmore, C. R. Reed and C. Turro, *Inorg. Chem.* , 2009, **48**, 4394.
17. B. G. Alberding, M. H. Chisholm, T. L. Gustafson, Y. Liu, C. R. Reed and C. Turro, *J. Phys. Chem. A*, 2010, **114**, 12675.
18. B. G. Alberding, M. H. Chisholm, Y.-H. Chou, Y. Ghosh, T. L. Gustafson, Y. Liu and C. Turro, *Inorg. Chem.*, 2009, **48**, 11187.
19. G. T. Burdzinski, M. H. Chisholm, P.-T. Chou, Y.-H. Chou, F. Feil, J. C. Gallucci, Y. Ghosh, T. L. Gustafson, M.-L. Ho, Y. Liu, R. Ramnauth and C. Turro, *Proc. Natl. Acad. Sci. USA*, 2008, **105**, 15247.
20. B. G. Alberding, M. H. Chisholm, J. C. Gallucci, Y. Ghosh and T. L. Gustafson, *Proc. Natl. Acad. Sci. USA*, 2011, **108**, 8152.
21. F. A. Cotton, C. Lin and C. A. Murillo, *Acc. Chem. Res.*, 2001, **34**, 759.
22. F. A. Cotton, C. Lin and C. A. Murillo, *Proc. Natl. Acad. Sci. USA*, 2002, **99**, 4810.
23. M. H. Chisholm and A. M. Macintosh, *Chem. Rev.*, 2005, **105**, 2949.
24. M. Köberl, M. Cokoja, B. Bechlars, E. Herdtweck and F. E. Kühn, *Dalton Trans.*, 2011, **40**, 11490.
25. F. A. Cotton, J.-Y. Jin, Z. Li, C. Y. Liu and C. A. Murillo, *Dalton Trans.*, 2007, 2328.
26. M. H. Chisholm, A. S. Dann, F. Dielmann, J. C. Gallucci, N. J. Patmore, R. Ramnauth and M. Scheer, *Inorg. Chem.*, 2008, **47**, 9248.
27. M. Köberl, M. Cokoja, W. A. Herrman and F. E. Kühn, *Dalton Trans.*, 2011, **40**, 6834.
28. J.-R. Li, A. A. Yakovenko, W. Lu, D. J. Timmons, W. Zhuang, D. Yuan and H.-C. Zhou, *J. Am. Chem. Soc.*, 2010, **132**, 17599.
29. C. Lin, J. D. Protsiewicz, E. T. Smith and T. Ren, *J. Chem. Soc., Chem. Commun.*, 1995, 2257.
30. C. Lin, J. D. Protsiewicz, E. T. Smith and T. Ren, *Inorg. Chem.*, 1996, **35**, 6422.
31. M. H. Chisholm and N. J. Patmore, *Dalton Trans.*, 2006, 3164.
32. M. J. Han, C. Y. Liu and P. F. Tian, *Inorg. Chem.*, 2009, **48**, 6347.
33. F. A. Cotton, Z. Li, C. Y. Liu and C. A. Murillo, *Inorg. Chem.*, 2007, **46**, 7840.
34. F. A. Cotton, Z. Li, C. A. Murillo, X. Wang, R. Yu and Q. Zhao, *Inorg. Chem.*, 2007, **46**, 3245.
35. F. A. Cotton, L. M. Daniels, I. Guimet, R. W. Henning, G. T. Jordan IV, C. Lin, C. A. Murillo and A. J. Schultz, *J. Am. Chem. Soc.*, 1998, **120**, 12531.
36. H. Adams, P. E. McHugh, M. J. Morris, S. E. Spey and P. J. Wright, *J. Organomet. Chem.*, 2001, **619**, 209.
37. M. Majumdar, S. K. Patra, M. Kannan, K. R. Dunbar and J. K. Bera, *Inorg. Chem.*, 2008, **47**, 2212.
38. B. Li, H. Zhang, L. Huynh, M. Shatruk and E. V. Dikarev, *Inorg. Chem.*, 2007, **46**, 9155.
39. H. P. M. M. Ambrosius, F. A. Cotton, L. R. Falvello, H. T. J. M. Hintzen, T. J. Melton, W. Schwotzer, M. Tomas and J. G. M. van der Linden, *Inorg. Chem.*, 1984, **23**, 1611.
40. F. A. Cotton, R. H. Niswander and J. C. Sekutowski, *Inorg. Chem.*, 1979, **18**, 1149.
41. G. 09.
42. F. A. Cotton, P. E. Fanwick, R. H. Niswander and J. C. Sekutowski, *Acta Chem. Scan. A*, 1978, **32**, 663.
43. B. G. Alberding, M. H. Chisholm, B. J. Lear, V. Naseri and C. R. Reed, *Dalton Trans.*, 2011, **40**, 10658.
44. M. H. Chisholm, *Phil. Trans. R. Soc. A*, 2008, **366**, 101.

45. T. H. M. Jonckers, S. van Miert, K. Cimanga, C. Bailly, P. Colson, M.-C. De Pauw-Gillet, H. van den Heuvel, M. Claeys, F. Lemière, E. L. Esmans, J. Rozenski, L. Quirijnen, L. Maes, R. Dommisse, G. L. F. Lemière, A. Vlietinck and L. Pieters, *J. Med. Chem.*, 2002, **45**, 3497.
46. P. S. Pandey and T. S. Rao, *Bioorg. Med. Chem. Lett.*, 2004, **14**, 129.
47. A. B. Brignole and F. A. Cotton, *Inorg. Synth.*, 1972, **13**, 81.
48. H. Fujita, R. Endo, A. Aoyama and T. Ichii, *Bull. Chem. Soc. Jpn.*, 1972, **45**, 1846.
49. G. M. Sheldrick, in *A program for absorption correction with the Siemens SMART system*, University of Gottingen, Germany, 1996.
50. G. M. Sheldrick, *Acta Cryst., Sect. A*, 1990, **46**, 467.
51. *SHELXTL program system version 5.1*, Bruker Analytical X-ray Instruments Inc., Madison, WI, 1998.
52. C. T. Lee, W. T. Yang and R. G. Parr, *Phys. Rev. B*, 1988, **37**, 785.
53. A. D. Becke, *J. Chem. Phys.*, 1993, **98**, 5648.
54. W. J. Hehre, L. Radom, P. v. R. Schleyer and J. A. Pople, *Ab initio Molecular Orbital Theory*, John Wiley & Sons, New York, 1986.
55. D. Andrae, U. Haeussermann, M. Dolg and H. Preuss, *Theor. Chim. Acta*, 1990, **77**, 123.
56. M. H. Chisholm, J. S. D'Acchioli and C. M. Hadad, *J. Clust. Sci.*, 2007, **18**, 27.